Reframing Whole-Body Angular Momentum: Exploring the Impact of Low-Pass Filtered Dynamic Local Reference Frames During Straight-Line and Turning Gaits

Junhao Zhang, Peter H. Veltink, *Senior Member, IEEE,*
and Edwin H. F. van Asseldonk, *Member, IEEE*

Abstract—**Accurately estimating whole-body angular momentum (WBAM) during daily activities may benefit from choosing a locally-defined reference frame aligned with anatomical axes, particularly during activities involving body turns. Local reference frames, potentially defined by pelvis heading angles, horizontal center of mass velocity (vCoM), or average angular velocity (Aω), can be utilized. To minimize the impact of inherent mediolateral oscillations of these frames, such as those caused by pelvis or vCoM rotation in the transverse plane, a low-pass filter is recommended. This study investigates how differences among global, local reference frames pre- and post-filtering affect WBAM component distribution across anatomical axes during straight-line walking and various turning tasks, which is lacking in the literature. Results highlighted significant effects of reference frame choice on WBAM distribution in the anteroposterior (AP) and mediolateral (ML) axes in all tasks. Specifically, expressing WBAM in the vCoM-oriented local reference frame yielded significantly lower (or higher) WBAM in the AP (or ML) axes compared to pelvis-oriented and Aω-oriented frames. However, these significant differences disappeared after employing a low-pass filter to local reference frames. Therefore, employing low-pass filtered local reference frames is crucial to enhance their applicability in both straight-line and turning tasks, ensuring more precise WBAM estimates. In applications that require expressing anatomical axes-dependent biomechanical parameters in a local reference frame, pelvis- and vCoM-oriented frames are more practical compared to the Aω-oriented frame, as they can be determined by a reduced optical marker set or inertial sensors in future applications when the whole-body kinematics is not available.**

Index Terms—**Whole-body angular momentum, local reference frame, turning gaits, anatomical axes, biomechanical measures.**

I. INTRODUCTION

WHOLE-BODY angular momentum (WBAM) with respect to the center of mass (CoM) plays an important role in human balance control. In stable straight-line walking tasks, it was found to be highly regulated throughout the walking cycle about all three anatomical axes, following a standard pattern [1], [2], [3]. Previous research has demonstrated how humans regulate their WBAM in challenging tasks, such as on uneven and unpredictable terrain [4], during stair ascent and descent [5], sloped walking [6], turning tasks [7], [8], and coping with external perturbations [9], [10], [11]. Humans continuously adjust their WBAM from standard patterns to maintain balance, which suggests the potential to assess balance by quantifying deviations from these usual patterns [12]. WBAM was also found to have close correlations to step placement [13]. It could help improve the foot placement estimation by considering the rotation momentum of the body rather than treating the body as a point mass [14]. Moreover, understanding WBAM can contribute to the development of assistive devices to restore efficient walking behavior during daily life [15], [16], [17]. All these attributes make WBAM a good option to extract an indicator of balance during daily life tasks.

WBAM is commonly interpreted in anatomical axes to enhance the understanding of balance performance across different anatomical dimensions, as demonstrated in previous studies [1], [2], [3]. This requires expressing WBAM in a suitable reference frame aligned with anatomical axes for reliable estimates during daily-life tasks. Previous research has used global reference frames (lab-fixed frames) and dynamic local reference frames (rotating with the body). In straight-line walking or running tasks, a global reference frame is usually

used where the axes of a global reference frame are fixed, such as the ones used for an optical motion capture system or OpenSim [18]. The anatomical axes are assumed to be fixed and aligned with the axes of the global reference frame. However, for activities involving body turns, anatomical axes also rotate with body direction. Measurements from a global reference frame lack anatomical significance in such cases. Therefore, it is often advisable to employ a dynamic local reference frame which aligns with the fixed anatomical axes in straight-line tasks and rotating anatomical axes in turning tasks [19].

Various dynamic local reference frames have been used during turning gaits. The vertical axis of a dynamic local reference frame is usually aligned with the global vertical axis, that is, a dynamic local reference frame is only a rotation of the global reference frame about the vertical axis [20]. For instance, dynamic local reference frames oriented by the pelvis heading [8], [21], or the horizontal center of mass velocity (vCoM) [7], [22] were found to be frequently used in literature to express WBAM in different anatomical axes in turning gaits. Both are continuous local reference frames as the directions of their axes are determined by the instantaneous pelvis heading angle or vCoM. Other local reference frames have been used to assess other biomechanical measures such as the ground reaction force (GRF), which could also be potentially suitable for expressing WBAM. For example, Mohamed Refai et al. [23] used a local reference frame which was defined by a vertical axis, and the line between the beginning and end positions of the swing foot for each step. Since this local reference frame changes with each step—its forward axis shifts from the direction of the current swing foot to that of the con-tralateral swing foot at heel strike—discontinuity may occur between steps. This discontinuity leads to discontinuity in the estimated GRF along horizontal axes, which may influence its interpretation. In [24], a finite-difference method based on the position of the whole-body or pelvis CoM at different time intervals was used to define local reference frames for expressing horizontal GRF. The authors concluded that it is better to choose two-time intervals, similar to the definition of vCoM-oriented local reference frame, to differentiate the position, as larger intervals result in larger discontinuities in the local reference frames. Therefore, continuous local reference frames are recommended for a smooth transition of WBAM between steps. Although various dynamic local reference frames have been used in literature, a comprehensive explanation of the distinctions between different dynamic local reference frames was barely studied in the literature.

The choice of reference frame has been demonstrated to alter interpretations of the gait variables during turning gaits. Ho et al. [25] found that different dynamic local reference frames had a significant influence on the resulting step length, step width, anteroposterior (AP) and mediolateral (ML) margin of stability (MoS) during turning gaits. However, the dif-ferences among WBAM expressed in various dynamic local reference frames have not been addressed in the literature. This oversight complicates comparisons between studies, as varia-tions in WBAM among different studies could be attributed solely to the choice of reference frame.

An ideal dynamic local reference frame should provide stable and anatomically relevant axes in both straight-line and turning tasks. However, in our previous study [26], dynamic local reference frames were observed to have oscillations in the mediolateral direction due to the rotation of the pelvis or vCoM in the transverse plane with a frequency equal to the stride frequency, which is referred to as mediolateral oscillations in this paper. Although it is an expected movement during gaits, it may lead to a less stable and anatomically relevant local reference frame. This misalignment may result in extra uncertainty in interpreting the distribution of WBAM components along different axes. Additionally, choosing a local reference frame that rotates with the mediolateral oscil-lations would also eliminate detailed biomechanical features related to these oscillations. Our previous research [26] sug-gested using a low-pass filter to remove the mediolateral oscillations, aiming to provide a more stable, yet anatomically relevant reference frame in both straight-line and turning tasks. It is noted that aligning with the anatomical axes during straight-line tasks equals aligning with the global reference frame since the anatomical axes are assumed to be fixed and align with the axes of the global frame as mentioned before.

Except for the ability to remove the mediolateral oscilla-tions, the low-pass filter should also avoid excessive smoothing in turning tasks. The low-pass filter should have a small impact on the alignment of the local reference frame during the stride cycles before or after turning while also preserving the turning features during the turning period. The cut-off frequency should be lower than the stride frequency and higher than the turning frequency (the frequency of changing the walking direction). However, it is uncertain how much low-pass filter-ing the local reference frame would impact the distribution of WBAM components around different anatomical axes in both straight-line and turning tasks.

The purpose of the present study was to answer the fol-lowing question: How do the differences among the global reference frame and various non-low-pass filtered (Non-LP) and low-pass filtered (LP) local reference frames influence the distribution of WBAM components around different anatomi-cal axes? This paper included a straight-line walking task and several turning tasks with different curvatures. Among various dynamic local reference frames, we chose the pelvis-oriented and vCoM-oriented dynamic local reference frames which were commonly used in literature. Additionally, we introduced an Aω-oriented dynamic local reference frame. It is defined by the transverse plane body rotation angle calculated by integrating the average angular velocity of the body [27], which is averaged over all segments at any moment in time. Although the Aω-oriented frame has not been used in literature, the rotation angle calculated by integrating the average angular velocity has been utilized as a representative of the total body orientation in different planes in previous studies [28], [29]. Therefore, the Aω-oriented frame may be a suitable local reference frame which is more anatomically relevant than other local reference frames as it is determined by considering the average orientation of all the body seg-ments. Our analysis began by investigating the frame angle differences across the global reference frame, as well as
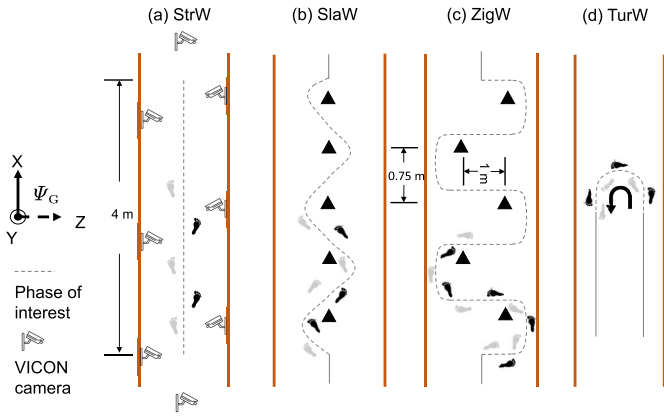
Fig. 1. Schematic diagrams for different tasks, (a) straight-line walking (StrW), (b) slalom walking (SlaW), (c) Zig-zag walking (ZigW), (d) walking with 180-degree turn (TurW). Five pylons were placed in a line on the floor with a forward distance of 0.75 m for the SlaW task to guide the participants, they performed turns less than 90 degrees. For the ZigW task, these five pylon were placed at two sides of the walkway with a parallel distance of 1 m and a forward distance of 0.75m, and participants performed approximately a 90-degree turn. The phase of interest of each task was denoted by a dashed grey line.

various Non-LP and LP local reference frames. Subsequently, we compared the differences among the WBAM expressed in these reference frames to answer the research question. Finally, we provided insightful explanations of the distinctions between different reference frames and offered guidance on selecting an appropriate one. The requirements of being an appropriate reference frame include aligning well with the anatomical axes in both straight-line and turning tasks without having substantial mediolateral oscillations, and being easy to calculate with optical data and future applications using inertial measurement unit (IMU) data.

II. METHOD

A. Setup

Ten healthy participants, including four females and six males enrolled in the experiments with age 27(3) years old, weight 72.4(10.8) kg, height 1.73(0.12) m, which were expressed as mean (standard deviation, SD). Research procedures were in accordance with the Declaration of Helsinki and were approved by the Ethics Committee Computer & Information Science of the University of Twente (No. 230257). Informed consent was received from all participants.

Participants were asked to perform several tasks at their normal walking speed and stride frequency, including walking along a straight line (StrW), slalom walking (SlaW), Zig-zag walking (ZigW), and walking with 180-degree turn (TurW) tasks, as shown in Fig. 1. The mean (SD) of walking speeds and stride frequencies for StrW, SlaW, ZigW and TurW tasks are 1.17 (0.16) m/s and 0.91 (0.06) Hz, 1.09 (0.15) m/s and 0.80 (0.05) Hz, 1.04 (0.13) m/s and 0.81 (0.05) Hz, and 1.10 (0.15) m/s and 0.87 (0.06) Hz, respectively. There are two turning strategies during human walking, the step-turn and spin-turn strategies [30]. The step-turn strategy was more frequently used than the spin-turn strategy for both healthy people and people with diseases [31]. In this paper, we decided to maintain the same turning strategy and all participants were instructed
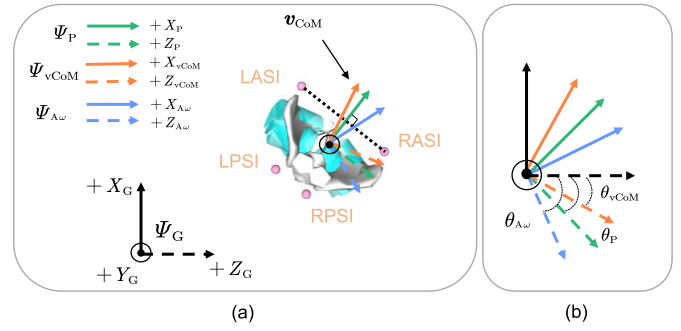

Fig. 2. Visualization of the global 9_G (black), pelvis-oriented 9_P (green), vCoM-oriented 9_{vCoM} (orange) and Aω-oriented $9_{A\omega}$ (blue) dynamic local reference frames. (b) Rotation angles between global and dynamic local reference frames, where the angle of the counterclockwise rotation as shown in the figure was denoted as negative values.

to use the step-turn strategy to perform a normal turn that is more common in daily life [31], [32]. All tasks were repeated 3 times. The 3-D kinematics of the participants was recorded using an optical motion capture system (VICON, Oxford, UK) with a sample rate of $f_s = 100$ Hz. Optical markers were placed according to the Plug-in Gait protocol plus one marker at each 5th metatarsal phalanx, including 41 markers on the subject's skin.

B. Data Preprocessing

Data processing was carried out using Matlab (R2023b, MathWorks). Raw marker position data were filtered using a zero-phase second-order (biquad), 6 Hz Butterworth low-pass filter. A full-body model consisting of 22 segments was scaled for each participant using OpenSim 4.3. The OpenSim *inverse kinematics tool* and *Analyze tool* were employed to calculate the 3-D segment kinematics of each participant, including the positions and velocities of the whole-body and segmental CoMs, orientations and angular velocities of all segments expressed in the global reference frame.

C. The Definitions of Reference Frames

As shown in Fig. 2(a), the $+X_G$ of the global reference frame was the walking direction of the StrW task, the vertical axis $+Y_G$ pointed upwards, and $+Z_G$ pointed horizontally and was perpendicular to the walking direction, as defined in the OpenSim [33]. The vertical axes ($+Y_P$, $+Y_{vCoM}$, and $+Y_{A\omega}$) of all dynamic local reference frames were aligned with the global vertical axis. The pelvis-oriented reference frame Ψ_P [8] was defined by using the vector from LASI marker to RASI marker to determine the ML axis ($+Z_P$), and the right-handed cross-product of $+Y_P$ and $+Z_P$ was taken as the AP axis ($+X_P$). The AP axis ($+X_{vCoM}$) of the vCoM-oriented reference frame Ψ_{vCoM} [7] was defined by the vector of the instantaneous velocity of the whole-body CoM in the transverse plane, and the ML axis ($+Z_{vCoM}$) was determined by the cross-product of $+X_{vCoM}$ and $+Y_{vCoM}$. The whole-body CoM velocity was obtained from the output of the *Analyze tool*. The Aω-oriented reference frame $\Psi_{A\omega}$ was defined by rotating the global reference frame with the transversal plane body orientation angle. The transversal plane body orientation angle was calculated by integrating the vertical component

of the average angular velocity [27] of the body with a time interval of $1/f_s$ s. The average angular velocity of the body was obtained by averaging over all segments, which was

$$^{\mathrm{G}}\boldsymbol{\omega}_{\mathrm{ave}} = \frac{^{\mathrm{G}}\boldsymbol{H}}{^{\mathrm{G}}\boldsymbol{I}} \tag{1}$$

where $^{\mathrm{G}}\boldsymbol{H}$ and $^{\mathrm{G}}\boldsymbol{I}$ are the WBAM and whole-body inertia tensor with respect to the whole-body CoM, respectively. The vertical component of the average angular velocity of the body was obtained by $^{\mathrm{G}}\omega_{\mathrm{ave}} = {^{\mathrm{G}}\boldsymbol{\omega}_{\mathrm{ave}}} \left(0 \; 1 \; 0\right)^T$. $^{\mathrm{G}}\boldsymbol{H}$ and $^{\mathrm{G}}\boldsymbol{I}$ were expressed in the global reference frame Ψ_{G} defined in Fig. 1, and they were calculated as

$$^{\mathrm{G}}\boldsymbol{H} = \sum_{j=1}^{22} {^{\mathrm{G}}\boldsymbol{H}_{\mathrm{CoM},j}}$$
$$= \sum_{j=1}^{22} \left[\left({^{\mathrm{G}}\boldsymbol{r}_{\mathrm{CoM},j}} - {^{\mathrm{G}}\boldsymbol{r}_{\mathrm{CoM}}} \right) \right.$$
$$\left. \times m_j \left({^{\mathrm{G}}\boldsymbol{v}_{\mathrm{CoM},j}} - {^{\mathrm{G}}\boldsymbol{v}_{\mathrm{CoM}}} \right) + {^{\mathrm{G}}\boldsymbol{I}_j} {^{\mathrm{G}}\boldsymbol{\omega}_j} \right] \tag{2}$$

$$^{\mathrm{G}}\boldsymbol{I} = \sum_{j=1}^{22} {^{\mathrm{G}}\boldsymbol{I}_{\mathrm{CoM},j}}$$
$$= \sum_{j=1}^{22} \left[m_j \cdot {^{\mathrm{G}}\tilde{\boldsymbol{r}}_{\mathrm{CoM},j/\mathrm{CoM}}^{\mathrm{T}}} {^{\mathrm{G}}\tilde{\boldsymbol{r}}_{\mathrm{CoM},j/\mathrm{CoM}}} + {^{\mathrm{G}}\boldsymbol{I}_j} \right] \tag{3}$$

where j represents each body segment, a full-body model consisting of 22 segments [34] was used $^{\mathrm{G}}\boldsymbol{H}_{\mathrm{CoM},j}$ and $^{\mathrm{G}}\boldsymbol{I}_{\mathrm{CoM},j}$ are the segmental angular momentum and inertia tensor of j-th segment with respect to the whole-body CoM, respectively. $^{\mathrm{G}}\boldsymbol{r}_{\mathrm{CoM},j}$ and $^{\mathrm{G}}\boldsymbol{r}_{\mathrm{CoM}}$ are the positions of j-th segment and the whole-body CoMs, respectively, and $^{\mathrm{G}}\boldsymbol{\omega}_j$ represents the angular velocity of each segment. $^{\mathrm{G}}\boldsymbol{v}_{\mathrm{CoM},j}$ and $^{\mathrm{G}}\boldsymbol{v}_{\mathrm{CoM}}$ are the velocities of j-th segment and the whole-body CoMs, respectively. Whole-body CoM position and velocity were calculated as the mass-weighted sum of the CoM positions and velocities of all segments. Body segment inertial parameters (i.e., mass m_j and inertia tensor $^{\mathrm{G}}\boldsymbol{I}_j$ with respect to the segment CoM) were calculated using procedures described by de Leva [35]. $^{\mathrm{G}}\boldsymbol{I}_{\mathrm{CoM},j}$ is obtained from the parallel-axis theorem, where $^{\mathrm{G}}\tilde{\boldsymbol{r}}_{\mathrm{CoM},j/\mathrm{CoM}}$ is the skew-symmetric matrix of the relative position vector from whole-body CoM to j-th segment CoM, i.e., $\left({^{\mathrm{G}}\boldsymbol{r}_{\mathrm{CoM},j}} - {^{\mathrm{G}}\boldsymbol{r}_{\mathrm{CoM}}} \right)$. The skew matrix of a vector $\boldsymbol{\rho} = \left[\rho_x, \rho_y, \rho_z \right]$ is defined as:

$$\tilde{\boldsymbol{\rho}} = \begin{bmatrix} 0 & -\rho_z & \rho_y \\ \rho_z & 0 & -\rho_x \\ -\rho_y & \rho_x & 0 \end{bmatrix} \tag{4}$$

Please refer to equation (5.51) in [36] for the parallel-axis theorem in (3) if it is accessible for readers, otherwise one can refer to equation (14) in [37] for a similar calculation. All measures are now given in the global reference frame Ψ_{G}. The inertia tensor of each body segment was first given in the body-fixed reference frame of each segment ($\Psi_{\mathrm{B},j}$), which is defined in OpenSim and moves along with the segment. $^{\mathrm{G}}\boldsymbol{I}_j$ was then calculated as

$$^{\mathrm{G}}\boldsymbol{I}_j = {^{\mathrm{G}}\boldsymbol{R}_{\mathrm{B},j}} {^{\mathrm{B},j}\boldsymbol{I}_j} \left({^{\mathrm{G}}\boldsymbol{R}_{\mathrm{B},j}} \right)^{\mathrm{T}} \tag{5}$$

where $^{\mathrm{B},j}\boldsymbol{I}_j$ is the inertia tensor of each body segment defined in its body-fixed reference frame ($\Psi_{\mathrm{B},j}$), which is a fixed value. $^{\mathrm{G}}\boldsymbol{R}_{\mathrm{B},j}$ is the rotation matrix between $\Psi_{\mathrm{B},j}$ and Ψ_{G}, and was calculated in OpenSim.

Our previous study [26] proposed a method to find the optimal cut-off frequency and filter order for both StrW and TurW tasks. Using the same data collected in this paper, a second-order low-pass filter with a cut-off frequency of 0.5 Hz was found to be optimal in filtering out oscillations for both StrW and TurW tasks while also preserving the turning features during the turning period of the TurW task. As explained in the Introduction, the requirement for a suitable cut-off frequency is lower than the stride frequency and higher than the turning frequency (if applicable). All participants were observed to take 3 to 4 strides for the SlaW task and 5 to 6 strides for the ZigW task to complete a full cycle of changing direction, thus the turning frequencies of both tasks are 1/3∼1/4 and 1/5∼1/6 of the stride frequency. A frequency of 0.5 Hz meets the requirement of being lower than the stride frequency and higher than the turning frequency. Therefore, we applied the same low-pass filter as used in the StrW and TurW tasks.

This low-pass filter was implemented to the frame angles of a dynamic local reference frame to generate a low-pass filtered dynamic local reference frame The difference between global and dynamic local reference frames could be represented by a rotation angle (θ_{P}, θ_{vCoM} and $\theta_{\mathrm{A}\omega}$), where clockwise rotation was denoted by negative angles, as shown in Fig. 2(b). The frame angles of the global reference frame (θ_{G}) are always 0. The frame angles of the LP dynamic local reference frame[1] were defined as $\theta_{\mathrm{P(LP)}}$, $\theta_{\mathrm{vCoM(LP)}}$ and $\theta_{\mathrm{A}\omega\mathrm{(LP)}}$.

D. Calculation of WBAM

The WBAM with respect to the whole-body CoM was first calculated in the global reference frame by (2), and subsequently was transferred to different Non-LP and LP dynamic local reference frames by a rotation matrix between the global and each of the dynamic local reference frames. For instance, the WBAM expressed in the Non-LP Ψ_{P} was calculated as

$$^{\mathrm{P}}\boldsymbol{H} = {^{\mathrm{P}}\boldsymbol{R}_{\mathrm{G},y} \left(\theta_{\mathrm{P}} \right)} {^{\mathrm{G}}\boldsymbol{H}} \tag{6}$$

where $^{\mathrm{P}}\boldsymbol{R}_{\mathrm{G},y} \left(\theta_{\mathrm{P}} \right)$ is the rotation matrix between Ψ_{G} and Ψ_{P}, representing a rotation around the vertical axis ($+Y_{\mathrm{P}}$) by θ_{P}. All WBAM were normalized for individual participants by dividing them through a scaling factor based on the participant's mass (M, kg), walking speed (V, m/s), and leg length (L, m), resulting in a unitless angular momentum measure [1].

There are two important considerations to be highlighted. Firstly, it is crucial to note that the difference between the WBAM estimated in global and local reference frames only involves a rotation around the vertical axis. Consequently, the magnitude of WBAM and the component of WBAM around

---

[1]Non-LP and LP local reference frames were both defined by the 6 Hz-low-pass-filtered marker data and the inverse kinematics derived from OpenSim. 'Non-LP' and 'LP' indicate whether the local reference frame is low-pass filtered by the zero-phase second-order Butterworth low-pass filter with a 0.5 Hz cut-off frequency.
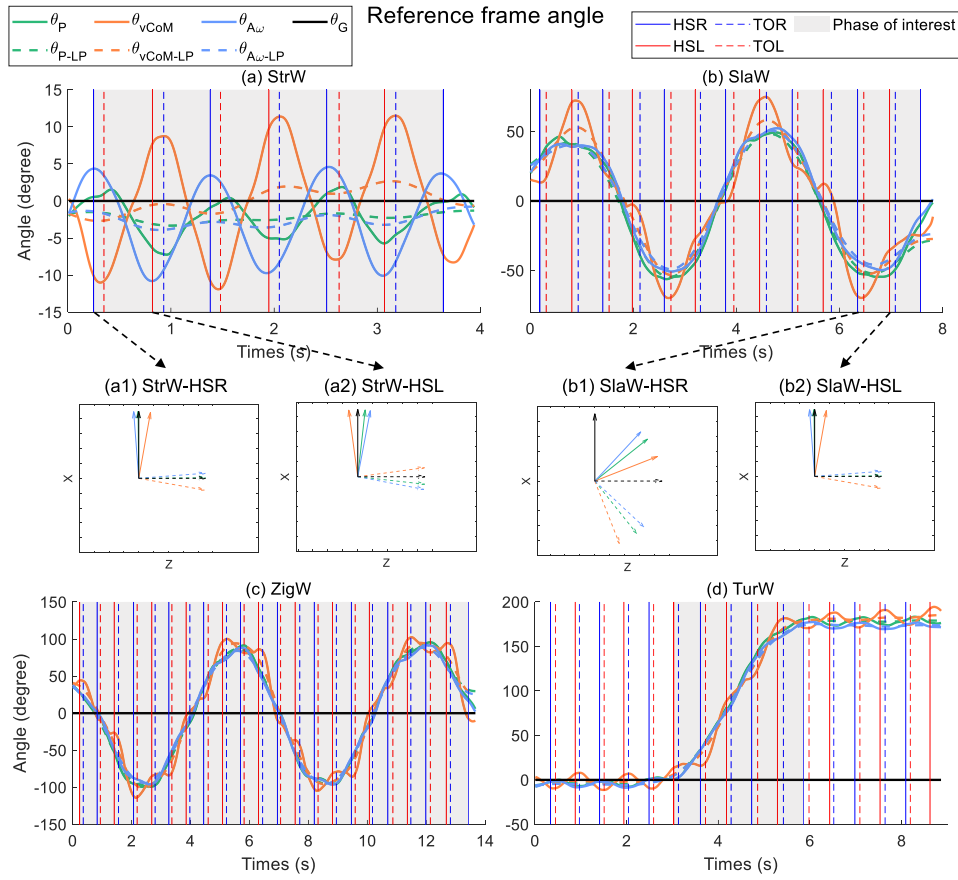
Fig. 3. Frame angles of the global θ_G, pelvis-oriented θ_P (green, solid), vCoM-oriented θ_{vCoM} (orange, solid), Aω-oriented $\theta_{A\omega}$ (blue, solid) dynamic local reference frames and their low-pass filtered ones (dashed lines with the same color) for a participant performing (a) StrW, (b) SlaW, (c) ZigW, and (d) TurW tasks. In these plots, the light-gray area represents the phase of interest. The moments of heel strike right (HSR), heel strike left (HSL), toe-off right (TOR) and toe-off left (TOL) are displayed as vertical blue, red, blue-dashed, and red-dashed lines, respectively. Furthermore, (a1-b2) shows an example of the $+X$ and $+Z$ axes of the three local reference frames at the moment of HSR and HSL in the StrW and SlaW tasks, respectively.

the vertical axis remain consistent across different reference frames. Only the components of WBAM around X (AP axis, perpendicular to the frontal plane) and Z axes (ML axis, perpendicular to the sagittal plane) are different, and therefore, compared in our paper. For simplification, we used AP and ML WBAM to indicate the components of WBAM around X and Z axes in the following text. Secondly, it is worth mentioning that one can also directly calculate the WBAM with respect to a local reference frame by measuring all variables in that frame. This approach mirrors the method we used where the WBAM is first calculated in the global reference frame and then transferred to the local reference frame. This approach is detailed in the Appendix for further clarification.

Our analysis was conducted during the phase of interest [8] of each task as shown in Fig. 1. For the StrW task, we focused on the phase of interest when the participant's CoM position was within the central 4 meters of the walkway, bounded by the first and last heel strikes. In other turn tasks, the turn phase (phase of interest) was determined using the pelvis heading angle. The pelvis heading angle was the same as θ_P. We identified the maximum and minimum pelvis heading angles within stride cycles during StrW trials, averaging them to establish person-specific positive and negative thresholds, respectively. The heel strike before the pelvis threshold was

reached was the start of the turn phase. The end of the turn phase was defined by the first heel strike that occurred after the pelvis heading angle was reduced below the thresholds.

E. Evaluation Measures and Statistics

In order to provide insights of the global and various dynamic local reference frames, we conducted an analysis of the discrepancies in frame angles among these different reference frames. We calculated the root mean square (RMS) of the frame angle differences between the global, and various Non-LP or LP dynamic local reference frames (RMSθ_{G-P}, RMSθ_{G-vCoM}, RMS$\theta_{G-A\omega}$) in the StrW task to investigate how the low-pass filter improved the alignment between local reference frames and the anatomical axes. Since we do not have a gold standard for anatomical axes, especially in turning tasks, we compared the RMS frame angle differences across various Non-LP and LP dynamic local reference frames (RMS$\theta_{P-A\omega}$, RMSθ_{P-vCoM}, RMS$\theta_{A\omega-vCoM}$) as evaluation measures to analyse their distinctions in all tasks.

Subsequently, we compared the AP and ML WBAM expressed in the global reference frame and various Non-LP and LP dynamic local reference frames. This analysis aimed to investigate how the differences among the global reference
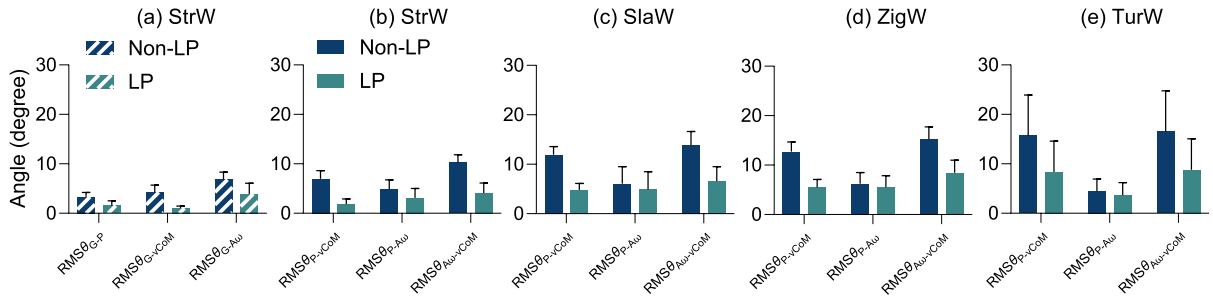
Fig. 4. (a) The RMS frame angle differences between the global, and various Non-LP or LP dynamic local reference frames (RMSθ_{G-P}, RMSθ_{G-vCoM}, RMS$\theta_{G-A\omega}$) in the StrW task, (b-e) the RMS frame angle differences across various Non-LP and LP dynamic local reference frames (RMS$\theta_{P-A\omega}$, RMSθ_{P-vCoM}, RMS$\theta_{A\omega-vCoM}$) in the StrW, SlaW, ZigW and TurW tasks. Mean values with standard deviation error bars over all trails and participants are displayed.

frame and various Non-LP and LP local reference frames influenced the distribution of WBAM components around different anatomical axes. The normalized RMS (NRMS, %) of the AP and ML WBAM differences between the global, and various Non-LP or LP dynamic local reference frames (NRMSH_{G-P}, NRMSH_{G-vCoM}, NRMS$H_{G-A\omega}$) were calculated in the StrW task, and the RMS of the AP and ML WBAM differences among various Non-LP and LP dynamic local reference frames (NRMS$H_{P-A\omega}$, NRMSH_{P-vCoM}, RMS$\theta_{A\omega-vCoM}$) were calculated in all tasks. They were all normalized by the range of the AP and ML WBAM expressed in their respective reference frames.

Additionally, linear mixed models were further used to test the effect of the reference frame on the distribution of WBAM components in the AP and ML axes before and after low-pass filtering. The statistical analysis was performed in RStudio (Posit Software, Boston, USA). Linear mixed models were fitted for the following outcome measures with the reference frame as the factor: maximum (Max), minimum (Min) and range of the AP and ML WBAM, which were extracted during each step. Random effects for the intercept and slope were included to take into account the participant effects. Post-hoc contrasts were tested for pair-wise comparisons between each pair of reference frames, and a Bonferroni correction was used to account for multiple comparisons. Significance was assessed at an alpha level of 0.05.

III. Results

A. Comparisons Before Low-Pass Filtering

In the strW task, all Non-LP dynamic local reference frames showed differences compared to the global reference frame (Fig. 3a) with an average of RMS frame angle difference of 4.8 (1.3) degrees (Fig. 4a). These frame angle differences resulted in an average of NRMS WBAM differences of 3.5 (1.2)% and 2.1 (1.0)% around the AP and ML axes (Figs. 6a and 7a), respectively. Significant differences in most WBAM outcome measures between the global and non-LP dynamic local reference frames (Table I) were observed, especially around the AP axis. Detailed distribution (Mean, SD) of the AP and ML WBAM outcome measures expressed in the global, various Non-LP and LP dynamic local reference frames can be found in the supplementary material.

Figs. 3a-d and 5a-d showed that during both the StrW and turning tasks, Non-LP Ψ_P and $\Psi_{A\omega}$ showed similarity in the frame angles and WBAM with only a slight difference, while Non-LP Ψ_{vCoM} showed a large variation compared to those of Non-LP Ψ_P and $\Psi_{A\omega}$. Ψ_{vCoM} exhibited a pronounced oscillatory motion around each side of Non-LP Ψ_P and $\Psi_{A\omega}$ within each step (see Fig. 3a1-b2). As displayed in Figs. 4, 6, 7b-e, RMS$\theta_{P-A\omega}$ had an average value of 5.4 (2.5) degrees, leading to an average NRMS$H_{P-A\omega}$ of only 2.3 (1.0)% and 2.8 (1.5)% in the AP and ML axes, respectively, across all tasks. RMSθ_{P-vCoM} and RMS$\theta_{A\omega-vCoM}$ had an average value of 11.8 (3.4) and 14.0 (3.8) degrees across all tasks, respectively. The average value of NRMSH_{P-vCoM} and NRMS$H_{A\omega-vCoM}$ across all tasks were 5.3 (2.2)% and 6.3 (2.2)% in the AP axis, 5.8 (2.1)% and 6.9 (2.5)% in ML axis, respectively. They were all much larger than those between Non-LP Ψ_P and $\Psi_{A\omega}$. Furthermore, the frame angle differences between Non-LP Ψ_P and $\Psi_{A\omega}$ had almost no significant influence in their pair-wise comparisons in both AP and ML WBAM outcome measures as shown in Table I, while those outcome measures extracted from Non-LP Ψ_{vCoM} were significantly different from those of Non-LP Ψ_P and $\Psi_{A\omega}$ in most conditions. Specifically, expressing WABM in Non-LP Ψ_{vCoM} underestimated the Max, Min and Range of the AP WBAM, and overestimated the Min and Range of the ML WBAM compared to Non-LP Ψ_P or $\Psi_A\omega$ (see Table I and the supplementary material).

B. Comparisons After Low-Pass Filtering

In the StrW task, the low-pass filter decreased the frame angle differences and WBAM differences between the global and all LP dynamic local reference frames (Figures 3a and 5a). The average value among RMSθ_{G-P}, RMSθ_{G-vCoM} and RMS$\theta_{G-A\omega}$ decreased to only 2.2 (1.2) degrees (Fig. 4a), and that among NRMSH_{G-P}, NRMSH_{G-vCoM} and NRMS$H_{G-A\omega}$ decreased to only 1.5 (0.9)% and 0.8 (0.5)% in the AP and ML axes, respectively (Fig. 6a and Fig. 7a). Table I indicated no significant differences in all AP and ML WBAM outcome measures between the global and various LP dynamic local reference frames.

Furthermore, the low-pass filter decreased the frame angle and WBAM differences among different LP dynamic local reference frames in both straight-line and turning tasks (Figs. 3a-d and 5a-d), especially between LP Ψ_{vCoM} and Ψ_P or
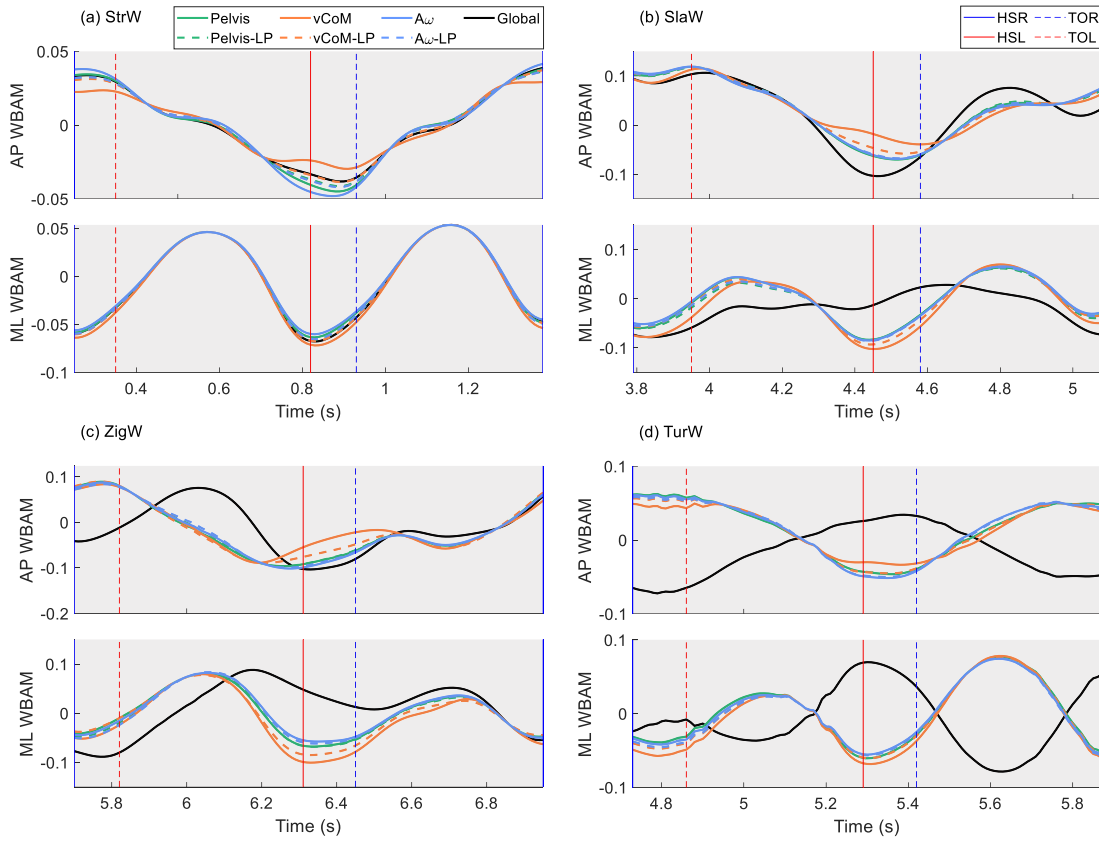
Fig. 5. The AP and ML WBAM expressed in the global (black, solid), pelvis-oriented (green, solid), vCoM-oriented (orange, solid), Aω-oriented (blue, solid) dynamic local reference frames and their low-pass filtered ones (dashed lines with the same color) for a participant performing (a) StrW, (b) SlaW, (c) ZigW, and (d) TurW tasks. Only one of the stride cycles (from HSR to the next HSR) within a trial was shown. The moments of HSR, HSL, TOR and TOL are displayed as vertical blue, red, blue-dashed, and red-dashed lines, respectively.
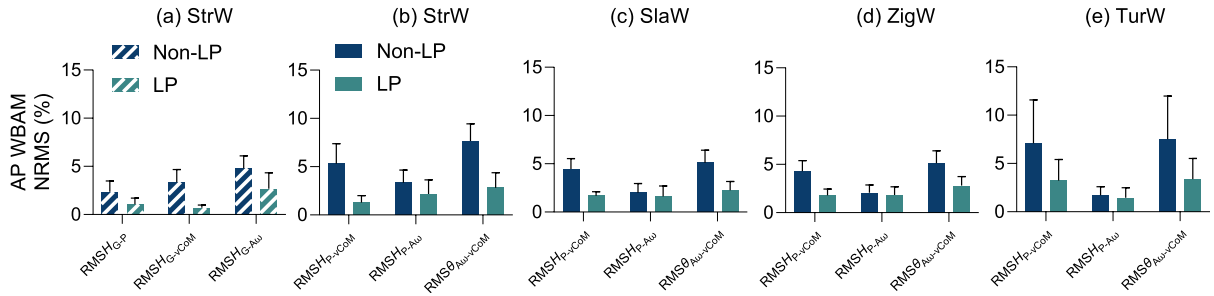

Fig. 6. (a) The NRMS differences of the AP WBAM between the global, and various Non-LP or LP dynamic local reference frames (NRMSH_{G-P}, NRMSH_{G-vCoM}, NRMS$H_{G-A\omega}$) in the StrW task, (b-e) the NRMS differences of the AP WBAM across various Non-LP and LP dynamic local reference frames (NRMS$H_{P-A\omega}$, NRMSH_{P-vCoM}, RMS$\theta_{A\omega-vCoM}$) in the StrW, SlaW, ZigW and TurW tasks. Mean values with standard deviation error bars over all trails and participants are displayed.

$\Psi_{A\omega}$. Figs. 4, 6, 7b-e indicated that after filtering, RMS$\theta_{P-A\omega}$, RMSθ_{P-vCoM}, RMS$\theta_{A\omega-vCoM}$ had an average value of 4.3 (2.6), 5.1 (2.5), and 7.0 (3.5) degrees, respectively, across all tasks. The average value of NRMS$H_{P-A\omega}$, NRMSH_{P-vCoM}, RMS$\theta_{A\omega-vCoM}$ across all tasks were 1.8 (1.1)%, 2.0 (1.0)% and 2.8 (1.4)% in the AP axis, 2.1 (1.4)%, 2.6 (1.4)% and 3.4 (1.9)% in ML axis, respectively. They were all smaller than those among Non-LP local reference frames. Almost no significant difference was found in AP and ML WBAM outcome measures among LP dynamic local reference frames as shown in Table I.

IV. DISCUSSION

This study investigated how the differences among the global reference frame and various Non-LP and LP local reference frames influence the distribution of WBAM components in different anatomical axes, during straight-line and various turning tasks. Firstly, our findings highlighted the significant impact of the mediolateral oscillations of various Non-LP local reference frames on the distribution of WBAM components during the StrW task. This prompts the use of a low-pass filter to filter out the mediolateral oscillations. Secondly, we found that among different local reference frames, Non-LP Ψ_P and $\Psi_{A\omega}$ displayed similar frame angles and WBAM during all tasks. The frame angles of Non-LP Ψ_{vCoM} showed a larger difference compared to those of Non-LP Ψ_P and $\Psi_{A\omega}$ due to the out-of-phase mediolateral oscillations of the horizontal vCoM around each of Ψ_P and $\Psi_{A\omega}$ within each step (see Fig. 3). The AP and ML components of the WBAM expressed in Non-LP Ψ_{vCoM} were also significantly different
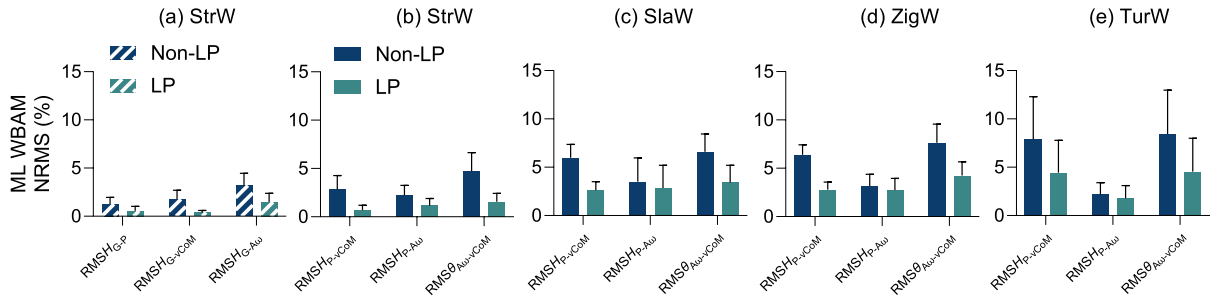
Fig. 7. (a) The NRMS differences of the ML WBAM between the global, and various Non-LP or LP dynamic local reference frames (NRMSH_{G-P}, NRMSH_{G-vCoM}, NRMS$H_{G-A\omega}$) in the StrW task, (b-e) the NRMS differences of the AP WBAM across various Non-LP and LP dynamic local reference frames (NRMS$H_{P-A\omega}$, NRMSH_{P-vCoM}, RMS$\theta_{A\omega-vCoM}$) in the StrW, SlaW, ZigW and TurW tasks. Mean values with standard deviation error bars over all trails and participants are displayed.

TABLE I

P-VALUES OF THE POST-HOC PAIR-WISE COMPARISONS OF AP AND ML WBAM OUTCOME MEASURES BETWEEN THE GLOBAL, AND VARIOUS NON-LP OR LP DYNAMIC LOCAL REFERENCE FRAMES IN THE STRW TASK, AND ACROSS VARIOUS NON-LP AND LP DYNAMIC LOCAL REFERENCE FRAMES IN THE STRW, SLAW, ZIGW AND TURW TASKS. A SIGNIFICANT DIFFERENCE WAS INDICATED BY * (p < 0.05). ↑ AND ↓ REPRESENT OVERESTIMATE AND UNDERESTIMATE THE WBAM OUTCOME MEASURES[1], RESPECTIVELY

		Comparison between global, and various Non-LP or LP dynamic local reference frames					
		StrW					
		G vs. P	G vs. vCoM	G vs. Aω	G vs. P(LP)	G vs. vCoM(LP)	G vs. Aω(LP)
AP WBAM	Max	0.019*↑	0.002*↓	0.001*↑	1.000	1.000	0.657
	Min	0.161	<0.001*↓	0.003*↑	1.000	1.000	1.000
	Range	0.004*↑	<0.001*↓	<0.001*↑	1.000	1.000	0.450
ML WBAM	Max	1.000	1.000	1.000	1.000	1.000	1.000
	Min	0.256	0.024*↑	0.008*↓	1.000	1.000	1.000
	Range	0.787	0.186	0.016*↓	1.000	1.000	1.000
		Comparison across various Non-LP or LP dynamic local reference frames					
		StrW					
		P vs. vCoM	P vs. Aω	Aω vs. vCoM	P(LP) vs. vCoM(LP)	P(LP) vs. Aω(LP)	Aω(LP) vs. vCoM(LP)
AP WBAM	Max	<0.001*↓	0.011*↑	<0.001*↓	1.000	0.568	0.503
	Min	0.001*↓	0.002*↑	<0.001*↓	1.000	1.000	1.000
	Range	<0.001*↓	<0.001*↑	<0.001*↓	1.000	0.111	0.074
ML WBAM	Max	1.000	1.000	1.000	1.000	1.000	1.000
	Min	0.002*↑	0.051	<0.001*↑	1.000	1.000	1.000
	Range	0.015*↑	0.171	<0.001*↑	1.000	1.000	0.053
		SlaW					
AP WBAM	Max	0.025*↓	1.000	0.013*↓	1.000	1.000	1.000
	Min	0.076	1.000	0.035*↓	1.000	1.000	1.000
	Range	0.009*↓	1.000	0.005*↓	1.000	1.000	1.000
ML WBAM	Max	1.000	1.000	1.000	1.000	1.000	1.000
	Min	<0.001*↑	1.000	0.003*↑	0.411	1.000	1.000
	Range	0.013*↑	1.000	0.005*↑	1.000	1.000	1.000
		ZigW					
AP WBAM	Max	0.002*↓	0.802	<0.001*↓	1.000	1.000	0.587
	Min	0.002*↓	1.000	0.002*↓	1.000	1.000	1.000
	Range	<0.001*↓	0.560	<0.001*↓	0.768	1.000	0.302
ML WBAM	Max	1.000	1.000	1.000	1.000	1.000	1.000
	Min	<0.001*↑	0.086	<0.001*↑	0.018*↑	1.000	0.017*↑
	Range	<0.001*↑	0.242	<0.001*↑	1.000	1.000	0.184
		TurW					
AP WBAM	Max	0.053	1.000	0.032*↓	0.425	1.000	0.435
	Min	0.197	1.000	0.080	1.000	1.000	1.000
	Range	0.019*↓	1.000	0.011*↓	0.910	1.000	0.752
ML WBAM	Max	1.000	1.000	1.000	1.000	1.000	1.000
	Min	0.016*↑	1.000	0.011*↑	0.129	1.000	0.190
	Range	0.043*↑	1.000	0.024*↑	0.545	1.000	0.560

[1] Overestimating (or underestimating) the WBAM outcome measure indicates that the absolute mean of the outcome measure of the latter comparison reference frame is higher (or lower) than that of the former. For example, the former and latter comparison reference frames in "G vs. P" are Ψ_G and Ψ_P, respectively. Detailed distribution (Mean, SD) of these AP and ML WBAM outcome measures expressed in the global, various Non-LP and LP dynamic local reference frames can be found in the supplementary material.

from those in Non-LP Ψ_P and $\Psi_A\omega$ in most conditions (see Fig. 5), due to these frame angle differences. Finally, the low-pass filter decreased the frame angle differences between the global and all LP dynamic local reference frames in the

StrW task, as well as among different LP dynamic local reference frames in all tasks. As a result, all LP dynamic local reference frames showed no significant differences in all AP and ML WBAM outcome measures in the StrW task compared to the global reference frame. Additionally, almost no significant difference was found in AP and ML WBAM outcome measures among various LP dynamic local reference frames.

In future studies, we suggest researchers to low-pass filter the local reference frames for expressing the WBAM in turning tasks. Our research revealed that the choice of reference frame significantly changed the distribution of WBAM around different axes before using the low-pass filter, that is, expressing WABM in Ψ_{vCoM} underestimated the AP WBAM and overestimated the ML WBAM compared to Ψ_P or $\Psi_{A\omega}$ (Table I). Therefore, it might be cumbersome for researchers to compare WBAM outcome measures from studies [7], [8], [21], [22] that used different local reference frames as the differences might just be a result of the difference in reference frames. The low-pass filter smoothed out all local reference frames by filtering out their mediolateral oscillations, diminishing the differences among them. No more significant difference in the outcome measures of AP and ML WBAM was found among them, which was highlighted in our study. Yet, this paper only investigated how the differences among Non-LP and LP local reference frames influence the distribution of WBAM components around different anatomical axes. It is of interest to underscore the importance of employing the low-pass filtered local reference frames by evaluating additional biomechanical measures that are usually assessed in anatomical axes. These biomechanical measures may include step length, step width, AP or ML MoS, CoM-center of pressure (CoP) distance [38], GRF [39], as well as the anticipated foot placement estimated by a foot placement estimator [14], etc.

Using low-pass filtered local reference frames not only helps standardize WBAM comparisons between studies by reducing variations due to the choice of different reference frames but also preserves the effects of mediolateral oscillations. We applied a low-pass filter with a 0.5 Hz cut-off frequency to smooth local reference frames defined by kinematic quantities such as the pelvis heading angle, horizontal CoM velocity, or the average transverse plane rotation angle of all body segments. Biomechanical parameters (e.g. the WBAM studied in this paper) that are related to these kinematic quantities are not low-pass filtered. This approach provides a more stable and anatomically relevant local reference frame during turning gaits which is not influenced by the mediolateral oscillations. Consequently, the critical effects of mediolateral oscillations on WBAM or other biomechanical measures can be maintained if expressing them in a low-pass filtered local reference frame, whereas using an oscillated local reference frame would obscure these details.

Considering the ease of calculation with optical data when a full-body marker set is not available, the LP Ψ_P and Ψ_{vCoM} were more advisable than the LP $\Psi_{A\omega}$ for expressing anatomical axes-dependent biomechanical parameters. In our work, Ψ_P was defined using only two markers, while Ψ_{vCoM} and $\Psi_{A\omega}$ relied on the whole-body inverse kinematics results,

thus a full-body marker set was required, such as the Plug-in Gait protocol used in this paper. However, reducing the marker set for estimating vCoM is possible [40], [41], [42]. Although $\Psi_{A\omega}$ could be a good representative of anatomical axes from a methodological point of view as it is determined by considering the average orientation of all the body segments in the transverse plane, the definition of $\Psi_{A\omega}$ always required the kinematics of all body segments, and it is difficult to estimate the whole-body kinematics using a reduced marker set. Moreover, the similarity between Non-LP (also LP) Ψ_P and $\Psi_{A\omega}$ indicated the former is an appropriate alternative of the latter. Our results also indicated that applying the low-pass filter to Ψ_P and Ψ_{vCoM} effectively eliminated their frame angle differences and no significant WBAM differences were found between them.

When using IMU data in future applications, the LP Ψ_P and Ψ_{vCoM} were also recommended over the LP $\Psi_{A\omega}$. The pelvis heading angle can be estimated with an IMU placed at the sacrum. Additionally, the vCoM can be estimated using a sacrum IMU [43] or a set of three IMUs [44]. However, $\Psi_{A\omega}$ demands a full-body set of IMUs [33] due to its requirement of whole-body kinematics, which typically requires an IMU at each body segment. Although learning-based methods for estimating whole-body kinematics using a reduced set of IMUs exist [45], [46], their performance heavily relies on the training motion database. This dependency can limit their applicability to scenarios not included in the database, and these methods remain more complex than those for estimating the pelvis heading angle and vCoM. As a result, regardless of whether optical data is employed as in this paper or IMU data in future applications, the LP $\Psi_{A\omega}$ may be less suitable than LP Ψ_P and Ψ_{vCoM} during turning tasks, as the whole-body kinematics is not always available. However, care should be taken when using a reduced marker set or IMUs to estimate vCoM, as the reduced accuracy may alter the comparable results between the LP Ψ_P and Ψ_{vCoM}.

While we recommend LP Ψ_P and Ψ_{vCoM} for expressing WBAM during turning tasks, the choice of reference frames should be carefully considered to support specific research questions in other applications and there are cases that other reference frames are more suitable. For studies that require the interpretation of other biomechanical measures in anatomical axes as mentioned earlier, LP Ψ_P and Ψ_{vCoM} may also be preferable when the whole-body kinematics is not available. In studies without turns, such as experiments on the treadmill, a fixed global reference frame is sufficient [25]. When anatomical relevance is prioritized over computational complexity, such as in studies focusing on body facing direction, the Non-LP $\Psi_{A\omega}$ should be considered as it is a good representative of anatomical axes as mentioned above. In cases where a walkway can be clearly defined [25], a walkway-fixed local reference frame can be denoted as an anatomical-related frame, which is free from mediolateral oscillations. It is noted that LP local reference frames might be expected to align more closely with the walkway-fixed frame than Non-LP frames. Conducting such comparisons could strengthen the recommendation for using an LP pelvis or vCoM-oriented local reference frame in scenarios where a defined path or walkway is not available.

Although the low-pass filter reduced the large difference between Ψ_{vCoM} and Ψ_{P} or $\Psi_{\mathrm{A}}\omega$, the cause of this difference is still interesting to be investigated, which has not been discussed in the literature. Tesio et al. [47], [48] found that the CoM trajectory had a figure-of-eight shape in the horizontal plane during straight-line tasks. At the moment of the heel strike of each step, the CoM oscillates laterally toward the stance foot, then starts to swing toward what is to become the next stance foot just after midstance [49]. The effect of this periodic movement of the CoM trajectory on the vCoM is that during each step, the mediolateral direction of the vCoM shifts from the stance foot to the swing leg, while the swing leg drives the pelvis to rotate in the opposite direction. As a result, the Non-LP Ψ_{vCoM} would oscillate out of phase around each side of Non-LP Ψ_{P} or $\Psi_{\mathrm{A}}\omega$, which could be observed from Fig. 3a1-a2. A similar explanation was provided in [50] through a detailed analysis of the phase difference between the transverse-plane linear and angular momenta in straight-line and turning gaits. This out-of-phase mediolateral oscillation of the vCoM led to much larger RMS$\theta_{\mathrm{P-vCoM}}$ and RMS$\theta_{\mathrm{A}\omega-\mathrm{vCoM}}$ than RMS$\theta_{\mathrm{P-A}\omega}$ in all the tasks before the low-pass filtering, especially around the heel strikes and early Single Stance (SS) phase, as shown from Fig. 3 and discussed in [50]. Consequently, the WBAM differences between Ψ_{vCoM} and Ψ_{P} or $\Psi_{\mathrm{A}}\omega$ are expected to be larger during Double Stance (DS) phases than during SS phases (see Fig. 5). This expectation was confirmed by our comparison of the RMS differences of the AP and ML WBAM across various Non-LP and LP dynamic local reference frames during the DS and SS phases (see **Table S2** in the supplementary material).

The optimal cut-off frequency was only determined based on all participants walking at their normal walking speeds and stride frequencies with a slow turning frequency, changing the condition may influence the choice of the cut-off frequency. In the case of more dynamic movements, the turning frequency may be higher than 0.5 Hz, a low-pass filter with this cut-off frequency would also filter out the turning. Additionally, for patients with very low stride frequencies, such as those with stroke or Parkinson's disease [51], 0.5 Hz might not be low enough to remove oscillations. However, for healthy adults, 0.5 Hz is lower than the stride frequency even when they walk at a slow walking speed [52]. Since most daily activities do not involve high-frequency turns, a 0.5 Hz cut-off frequency is generally suitable for most daily life scenarios.

Although comparing across turning tasks was not the central research question of this paper, there are important contrasts to share, across turning task analysis. The TurW task only included a 180-degree turn while the other two turning tasks were cyclic turns of less than or around 90 degrees. In the TurW task, turning around the vertical axis is more dominant than the mediolateral oscillations of local reference frames. Consequently, the mediolateral oscillations may not be as pronounced to the WBAM about the vertical axis, compared to the other two turning tasks. Accordingly, it is expected to observe that the WBAM outcome measures between the Non-LP Ψ_{vCoM} and Non-LP Ψ_{P} or $\Psi_{\mathrm{A}}\omega$ had the fewest significantly

different instances in the TurW task (see Table I). It is also expected that the frame angle, AP and ML WBAM differences between Ψ_{P} and $\Psi_{\mathrm{A}\omega}$ were smaller in the TurW task than in the SlaW and ZigW tasks (see Figs. 4, 6, 7e).

A. Limitations and Future Work

The primary limitation is that we do not have a golden standard for the anatomical axes during turning tasks, thus there is also a lack of a golden standard for the WBAM around different anatomical axes during turning tasks. This limits our ability to conclude whether the WBAM expressed in the suggested LP pelvis- or vCoM-oriented local reference frames accurately represents the true WBAM. It is important in future work to address this limitation through the establishment of a consensus on the golden standard for the WBAM around different anatomical axes during turning tasks. Another limitation is that although we have included more turning tasks than our previous work [26] and the low-pass filter has been proved to be applicable to the straight-line walking and various turning tasks, all participants performed these tasks with a normal speed. Faster or slower speeds may influence the performance of the low-pass filter as mentioned, and may vary the degree to which reference frames impact the WBAM interpretation. Moreover, different types of low-pass filters [53] could be considered in future applications.

Additionally, this study focused solely on step turns. When participants used the spin-turn strategy, characterized by turning on the ipsilateral limb [54], the distinctions between local reference frames observed in this paper may differ. For example, Ψ_{P} and $\Psi_{\mathrm{A}\omega}$ may be expected to be more aligned. While young healthy adults (the only population examined in this paper) prefer step turns, this preference declines in older populations. Older adults use a higher proportion of spin turns compared to younger adults. Therefore, an in-depth analysis of additional data collected from spin turns, from older adults and individuals with mobility impairments could provide further insight into the distinctions between local reference frames during turns. Finally, our work defined dynamic local reference frames using optical marker data and its inverse kinematics results, while in daily-life conditions, inertial measurement units (IMU) are more commonly used. Therefore, it is also essential to assess the complexity and accuracy of defining different dynamic local reference frames using IMU data.

V. Conclusion

In summary, our study highlights the significant impact of the choice of reference frame on the distribution of WBAM components around different anatomical axes during straight-line and turning tasks. Employing a low-pass filter with an optimal cut-off and filter order removed the inherent mediolateral oscillations of various local reference frames, which reduced their differences and provided more stable and anatomically relevant local reference frames. As a result, the significant differences in the distribution of WBAM around both AP and ML axes between global and local

$$
\begin{aligned}
{}^{\mathrm{L}}\boldsymbol{H} &= \sum_{j=1}^{22} {}^{\mathrm{L}}\boldsymbol{H}_{\mathrm{CoM},j} = \sum_{j=1}^{22} \left[{}^{\mathrm{L}}\boldsymbol{R}_{\mathrm{G}} \left({}^{\mathrm{G}}\boldsymbol{r}_{\mathrm{CoM},j} - {}^{\mathrm{G}}\boldsymbol{r}_{\mathrm{CoM}} \right) \times m_j \left({}^{\mathrm{G}}\boldsymbol{v}_{\mathrm{CoM},j} - {}^{\mathrm{G}}\boldsymbol{v}_{\mathrm{CoM}} \right) + \left({}^{\mathrm{L}}\boldsymbol{R}_{\mathrm{G}} {}^{\mathrm{G}}\boldsymbol{R}_{\mathrm{B},j} {}^{\mathrm{B}}\boldsymbol{I}_j{}^{\mathrm{B},j} \boldsymbol{R}_{\mathrm{G}} {}^{\mathrm{G}}\boldsymbol{R}_{\mathrm{L}} \right) \left({}^{\mathrm{L}}\boldsymbol{R}_{\mathrm{G}} {}^{\mathrm{G}}\boldsymbol{\omega}_j \right) \right] \\
&= \sum_{j=1}^{22} \left[{}^{\mathrm{L}}\boldsymbol{R}_{\mathrm{G}} \left({}^{\mathrm{G}}\boldsymbol{r}_{\mathrm{CoM},j} - {}^{\mathrm{G}}\boldsymbol{r}_{\mathrm{CoM}} \right) \times m_j \left({}^{\mathrm{G}}\boldsymbol{v}_{\mathrm{CoM},j} - {}^{\mathrm{G}}\boldsymbol{v}_{\mathrm{CoM}} \right) + {}^{\mathrm{L}}\boldsymbol{R}_{\mathrm{G}} \left({}^{\mathrm{G}}\boldsymbol{R}_{\mathrm{B},j} {}^{\mathrm{B}}\boldsymbol{I}_j \left({}^{\mathrm{G}}\boldsymbol{R}_{\mathrm{B},j} \right)^{\mathrm{T}} \right) {}^{\mathrm{G}}\boldsymbol{\omega}_j \right] \\
&= {}^{\mathrm{L}}\boldsymbol{R}_{\mathrm{G}} \sum_{j=1}^{22} \left[\left({}^{\mathrm{G}}\boldsymbol{r}_{\mathrm{CoM},j} - {}^{\mathrm{G}}\boldsymbol{r}_{\mathrm{CoM}} \right) \times m_j \left({}^{\mathrm{G}}\boldsymbol{v}_{\mathrm{CoM},j} - {}^{\mathrm{G}}\boldsymbol{v}_{\mathrm{CoM}} \right) + {}^{\mathrm{G}}\boldsymbol{I}_j {}^{\mathrm{G}}\boldsymbol{\omega}_j \right] = {}^{\mathrm{L}}\boldsymbol{R}_{\mathrm{G}} {}^{\mathrm{G}}\boldsymbol{H}
\end{aligned}
\tag{9}
$$

reference frames in the straight-line walking task, and among local reference frames in all tasks, were eliminated. Employing a low-pass filter enhances the applicability of dynamic local reference frames, ensuring more precise estimates of WBAM. In applications that require expressing anatomical axes-dependent biomechanical parameters in a local reference frame, local reference frames defined by the pelvis heading angle or the horizontal CoM velocity, are easier to apply compared to the $A\omega$-oriented frame since both of them could be determined by a reduced optical marker set or IMU when the whole-body kinematics is not available. Still, the choice of reference frames should be carefully considered to support specific research questions in other applications. These findings are expected to have practical implications for choosing a suitable dynamic local reference frame for getting reliable/accurate estimates of biomechanical measures during functional tasks in daily life.

Supplementary materials of this paper can be assessed in arXiv (https://github.com/JunHaoZhang1995/ReframingWABM.git).

APPENDIX A
THE CALCULATION OF WBAM WITH RESPECT TO A LOCAL REFERENCE FRAME

The WBAM with respect to a local reference frame was defined as

$$
\begin{aligned}
{}^{\mathrm{L}}\boldsymbol{H} \\
= \sum_{j=1}^{22} {}^{\mathrm{L}}\boldsymbol{H}_{\mathrm{CoM},j} \\
= \sum_{j=1}^{22} \left[\left({}^{\mathrm{L}}\boldsymbol{r}_{\mathrm{CoM},j} - {}^{\mathrm{L}}\boldsymbol{r}_{\mathrm{CoM}} \right) \times m_j \left({}^{\mathrm{L}}\boldsymbol{v}_{\mathrm{CoM},j} - {}^{\mathrm{L}}\boldsymbol{v}_{\mathrm{CoM}} \right) + {}^{\mathrm{L}}\boldsymbol{I}_j {}^{\mathrm{L}}\boldsymbol{\omega}_j \right]
\end{aligned}
\tag{7}
$$

where L represents one of the dynamic local reference frames, and all parameters were now measured in the local reference frame. We have

$$
{}^{\mathrm{L}}\boldsymbol{I}_j = {}^{\mathrm{L}}\boldsymbol{R}_{\mathrm{B},j} {}^{\mathrm{B}}\boldsymbol{I}_j \left({}^{\mathrm{L}}\boldsymbol{R}_{\mathrm{B},j} \right)^{\mathrm{T}}
$$
$$
{}^{\mathrm{L}}\boldsymbol{R}_{\mathrm{B},j} = {}^{\mathrm{L}}\boldsymbol{R}_{\mathrm{G}} {}^{\mathrm{G}}\boldsymbol{R}_{\mathrm{B},j}
\tag{8}
$$

Substituting (7) into (6) leads to (9), which is shown at the top of next page.

REFERENCES

[1] H. Herr and M. Popovic, "Angular momentum in human walking," *J. Experim. Biol.*, vol. 211, no. 4, pp. 467–481, Feb. 2008.

[2] V. Thielemans, P. Meyns, and S. M. Bruijn, "Is angular momentum in the horizontal plane during gait a controlled variable?" *Hum. Movement Sci.*, vol. 34, pp. 205–216, Apr. 2014.

[3] T. Negishi and N. Ogihara, "Regulation of whole-body angular momentum during human walking," *Sci. Rep.*, vol. 13, no. 1, p. 8000, May 2023.

[4] K. H. Yeates, A. D. Segal, R. R. Neptune, and G. K. Klute, "Balance and recovery on coronally-uneven and unpredictable terrain," *J. Biomechanics*, vol. 49, no. 13, pp. 2734–2740, Sep. 2016.

[5] A. K. Silverman, R. R. Neptune, E. H. Sinitski, and J. M. Wilken, "Whole-body angular momentum during stair ascent and descent," *Gait Posture*, vol. 39, no. 4, pp. 1109–1114, Apr. 2014.

[6] N. T. Pickle, J. M. Wilken, J. M. A. Whitehead, and A. K. Silverman, "Whole-body angular momentum during sloped walking using passive and powered lower-limb prostheses," *J. Biomechanics*, vol. 49, no. 14, pp. 3397–3406, Oct. 2016.

[7] L. A. Nolasco, A. K. Silverman, and D. H. Gates, "Whole-body and segment angular momentum during 90-degree turns," *Gait Posture*, vol. 70, pp. 12–19, May 2019.

[8] M. Tillman, J. Molino, and A. M. Zaferiou, "Frontal plane balance during pre-planned and late-cued 90 degree turns while walking," *J. Biomechanics*, vol. 141, Aug. 2022, Art. no. 111206.

[9] D. Martelli, V. Monaco, L. Bassi Luciani, and S. Micera, "Angular momentum during unexpected multidirectional perturbations delivered while walking," *IEEE Trans. Biomed. Eng.*, vol. 60, no. 7, pp. 1785–1795, Jul. 2013.

[10] M. van Mierlo, J. I. Ambrosius, M. Vlutters, E. H. F. van Asseldonk, and H. van der Kooij, "Recovery from sagittal-plane whole body angular momentum perturbations during walking," *J. Biomechanics*, vol. 141, Aug. 2022, Art. no. 111169.

[11] J. Zhang, M. van Mierlo, P. H. Veltink, and E. H. F. van Asseldonk, "Estimation of sagittal-plane whole-body angular momentum during perturbed and unperturbed gait using simplified body models," *Hum. Movement Sci.*, vol. 93, Feb. 2024, Art. no. 103179.

[12] K. Mombaur et al., "Control of motion and compliance," *Bioinspired Legged Locomotion*, pp. 135–346, Jan. 2017.

[13] J. K. Leestma, P. R. Golyski, C. R. Smith, G. S. Sawicki, and A. J. Young, "Linking whole-body angular momentum and step placement during perturbed human walking," *J. Experim. Biol.*, vol. 226, no. 6, Mar. 2023, Art. no. jeb244760.

[14] M. Millard, J. McPhee, and E. Kubica, "Foot placement and balance in 3D," *J. Comput. Nonlinear Dyn.*, vol. 7, no. 2, Jan. 2012, Art. no. 021015.

[15] S. D'Andrea, N. Wilhelm, A. K. Silverman, and A. M. Grabowski, "Does use of a powered ankle-foot prosthesis restore whole-body angular momentum during walking at different speeds?" *Clin. Orthopaedics Rel. Res.*, vol. 472, no. 10, pp. 3044–3054, Oct. 2014.

[16] C. Bayón et al., "Can momentum-based control predict human balance recovery strategies?" *IEEE Trans. Neural Syst. Rehabil. Eng.*, vol. 28, no. 9, pp. 2015–2024, Sep. 2020.

[17] S.-K. Yun and A. Goswami, "Momentum-based reactive stepping controller on level and non-level ground for humanoid robot push recovery," in *Proc. IEEE/RSJ Int. Conf. Intell. Robots Syst.*, Sep. 2011, pp. 3943–3950.

[18] S. L. Delp et al., "OpenSim: Open-source software to create and analyze dynamic simulations of movement," *IEEE Trans. Biomed. Eng.*, vol. 54, no. 11, pp. 1940–1950, Nov. 2007.

[19] H. Kainz, D. G. Lloyd, H. P. J. Walsh, and C. P. Carty, "Instantaneous progression reference frame for calculating pelvis rotations: Reliable and anatomically-meaningful results independent of the direction of movement," *Gait Posture*, vol. 46, pp. 30–34, May 2016.

[20] P. C. Fino, F. B. Horak, and C. Curtze, "Inertial sensor-based centripetal acceleration as a correlate for lateral margin of stability during walking and turning," *IEEE Trans. Neural Syst. Rehabil. Eng.*, vol. 28, no. 3, pp. 629–636, Mar. 2020.

[21] L. A. Nolasco, A. K. Silverman, and D. H. Gates, "Transtibial prosthetic alignment has small effects on whole-body angular momentum during functional tasks," *J. Biomechanics*, vol. 149, Mar. 2023, Art. no. 111485.

[22] L. A. Nolasco, J. Livingston, A. K. Silverman, and D. H. Gates, "The ins and outs of dynamic balance during 90-degree turns in people with a unilateral transtibial amputation," *J. Biomechanics*, vol. 122, Jun. 2021, Art. no. 110438.

[23] M. I. Mohamed Refai, B. F. van Beijnum, J. H. Buurke, and P. H. Veltink, "Portable gait lab: Tracking relative distances of feet and CoM using three IMUs," *IEEE Trans. Neural Syst. Rehabil. Eng.*, vol. 28, no. 10, pp. 2255–2264, Oct. 2020.

[24] B. C. Glaister, M. S. Orendurff, J. A. Schoen, and G. K. Klute, "Rotating horizontal ground reaction forces to the body path of progression," *J. Biomechanics*, vol. 40, no. 15, pp. 3527–3532, 2007.

[25] T. K. Ho, N. Kreter, C. B. Jensen, and P. C. Fino, "The choice of reference frame alters interpretations of turning gait and stability," *J. Biomechanics*, vol. 151, Apr. 2023, Art. no. 111544.

[26] J. Zhang, E. H. F. van Asseldonk, and P. H. Veltink, "Optimizing cut-off frequencies and filter orders for dynamic local reference frames for human gait analysis in straight-line and turning tasks," in *Proc. IEEE Int. Symp. Med. Meas. Appl.*, Jun. 2024, pp. 1–6.

[27] D. E. Orin, A. Goswami, and S.-H. Lee, "Centroidal dynamics of a humanoid robot," *Auto. Robots*, vol. 35, nos. 2–3, pp. 161–176, Oct. 2013.

[28] M. Pijnappels, I. Kingma, D. Wezenberg, G. Reurink, and J. H. van Dieën, "Armed against falls: The contribution of arm movements to balance recovery after tripping," *Exp. Brain Res.*, vol. 201, no. 4, pp. 689–699, Apr. 2010.

[29] S. M. Bruijn, L. H. Sloot, I. Kingma, and M. Pijnappels, "Contribution of arm movements to balance recovery after tripping in older adults," *J. Biomechanics*, vol. 133, Mar. 2022, Art. no. 110981.

[30] K. Hase and R. B. Stein, "Turning strategies during human walking," *J. Neurophysiol.*, vol. 81, no. 6, pp. 2914–2922, Jun. 1999.

[31] D. Conradsson, C. Paquette, J. Lökk, and E. Franzén, "Pre- and unplanned walking turns in Parkinson's disease—Effects of dopaminergic medication," *Neuroscience*, vol. 341, pp. 18–26, Jan. 2017.

[32] A. E. Patla, S. D. Prentice, C. Robinson, and J. Neufeld, "Visual control of locomotion: Strategies for changing direction and for going over obstacles," *J. Experim. Psychol., Human Perception Perform.*, vol. 17, no. 3, pp. 603–634, 1991.

[33] P. Slade, A. Habib, J. L. Hicks, and S. L. Delp, "An open-source and wearable system for measuring 3D human motion in real-time," *IEEE Trans. Biomed. Eng.*, vol. 69, no. 2, pp. 678–688, Feb. 2022.

[34] A. Rajagopal, C. L. Dembia, M. S. DeMers, D. D. Delp, J. L. Hicks, and S. L. Delp, "Full-body musculoskeletal model for muscle-driven simulation of human gait," *IEEE Trans. Biomed. Eng.*, vol. 63, no. 10, pp. 2068–2079, Oct. 2016.

[35] P. de Leva, "Adjustments to Zatsiorsky–Seluyanov's segment inertia parameters," *J. Biomechanics*, vol. 29, no. 9, pp. 1223–1230, Sep. 1996.

[36] H. Vallery and A. L. Schwab, *Advanced Dynamics*. Delft, The Netherlands: Delft Univ. Technology, 2017.

[37] A. R. Abdulghany, "Generalization of parallel axis theorem for rotational inertia," *Amer. J. Phys.*, vol. 85, no. 10, pp. 791–795, Oct. 2017.

[38] P. C. Fino, T. E. Lockhart, and N. F. Fino, "Corner height influences center of mass kinematics and path trajectory during turning," *J. Biomechanics*, vol. 48, no. 1, pp. 104–112, Jan. 2015.

[39] T. Yamaguchi, A. Suzuki, and K. Hokkirigawa, "Required coefficient of friction in the anteroposterior and mediolateral direction during turning at different walking speeds," *PLoS ONE*, vol. 12, no. 6, Jun. 2017, Art. no. e0179817.

[40] C. Forsell and K. Halvorsen, "A method for determining minimal sets of markers for the estimation of center of mass, linear and angular momentum," *J. Biomechanics*, vol. 42, no. 3, pp. 361–365, Feb. 2009.

[41] F. Yang and Y.-C. Pai, "Can sacral marker approximate center of mass during gait and slip-fall recovery among community-dwelling older adults?" *J. Biomechanics*, vol. 47, no. 16, pp. 3807–3812, Dec. 2014.

[42] K. L. Havens, T. Mukherjee, and J. M. Finley, "Analysis of biases in dynamic margins of stability introduced by the use of simplified center of mass estimates during walking and turning," *Gait Posture*, vol. 59, pp. 162–167, Jan. 2018.

[43] M. J. Floor-Westerdijk, H. M. Schepers, P. H. Veltink, E. H. F. van Asseldonk, and J. H. Buurke, "Use of inertial sensors for ambulatory assessment of center-of-mass displacements during walking," *IEEE Trans. Biomed. Eng.*, vol. 59, no. 7, pp. 2080–2084, Jul. 2012.

[44] M. I. Mohamed Refai, B.-J. F. van Beijnum, J. H. Buurke, and P. H. Veltink, "Portable gait lab: Instantaneous centre of mass velocity using three inertial measurement units," in *Proc. IEEE SENSORS*, Oct. 2020, pp. 1–4.

[45] Y. Huang, M. Kaufmann, E. Aksan, M. J. Black, O. Hilliges, and G. Pons-Moll, "Deep inertial poser: Learning to reconstruct human pose from sparse inertial measurements in real time," *ACM Trans. Graph.*, vol. 37, no. 6, pp. 1–15, Dec. 2018.

[46] F. J. Wouda, M. Giuberti, N. Rudigkeit, B.-J.-F. van Beijnum, M. Poel, and P. H. Veltink, "Time coherent full-body poses estimated using only five inertial sensors: Deep versus shallow learning," *Sensors*, vol. 19, no. 17, p. 3716, Aug. 2019.

[47] L. Tesio, V. Rota, C. Chessa, and L. Perucca, "The 3D path of body centre of mass during adult human walking on force treadmill," *J. Biomechanics*, vol. 43, no. 5, pp. 938–944, Mar. 2010.

[48] L. Tesio and V. Rota, "The motion of body center of mass during walking: A review oriented to clinical applications," *Frontiers Neurol.*, vol. 10, p. 999, Sep. 2019.

[49] S. M. Bruijn and J. H. van Dieën, "Control of human gait stability through foot placement," *J. Roy. Soc. Interface*, vol. 15, no. 143, Jun. 2018, Art. no. 20170816.

[50] M. Tillman, J. Molino, and A. M. Zaferiou, "Gait-phase specific transverse-plane momenta generation during pre-planned and late-cued 90 degree turns while walking," *Sci. Rep.*, vol. 13, no. 1, p. 6846, Apr. 2023.

[51] M. Tramontano et al., "Dynamic stability, symmetry, and smoothness of gait in people with neurological health conditions," *Sensors*, vol. 24, no. 8, p. 2451, Apr. 2024.

[52] E. M. Murtagh, J. L. Mair, E. Aguiar, C. Tudor-Locke, and M. H. Murphy, "Outdoor walking speeds of apparently healthy adults: A systematic review and meta-analysis," *Sports Med.*, vol. 51, no. 1, pp. 125–141, Jan. 2021.

[53] V. V. Shah et al., "Inertial sensor algorithms to characterize turning in neurological patients with turn hesitations," *IEEE Trans. Biomed. Eng.*, vol. 68, no. 9, pp. 2615–2625, Sep. 2021.

[54] P. Fino, C. Frames, and T. Lockhart, "Classifying step and spin turns using wireless gyroscopes and implications for fall risk assessments," *Sensors*, vol. 15, no. 5, pp. 10676–10685, May 2015.